ISSN 1063-7842, Technical Physics, 2021, Vol. 66, No. 4, pp. 635–641. © Pleiades Publishing, Ltd., 2021.
ISSN 1063-7842, Technical Physics, 2021. © Pleiades Publishing, Ltd., 2021.
Russian Text © The Author(s), 2021, published in Zhurnal Tekhnicheskoi Fiziki, 2021, Vol. 91, No. 4, pp. 620–626.

Magnetic Properties of the $DyMn_2O_5$–Mn_3O_4 Nanoparticle Composite

G. S. Patrin[a, c,*], M. M. Mataev[b], M. R. Abdraimova[b], Zh. I. Tursinova[b], A. T. Kezdikbaeva[d], Ya. G. Shiyan[a,c], and V. G. Plekhanov[a]

[a] *Siberian Federal University, Krasnoyarsk, 660041 Russia*

[b] *Kazakh National Women's Teacher Training University, Almaty, 050000 Kazakhstan*

[c] *Kirensky Institute of Physics, Krasnoyarsk Scientific Center, Siberian Branch, Russian Academy of Sciences, Krasnoyarsk, 660036 Russia*

[d] *Karaganda State University, Karaganda, 100028 Kazakhstan*

**e-mail: patrin@iph.krasn.ru*

Received June 23, 2020; revised November 6, 2020; accepted November 15, 2020

Abstract—The magnetic and resonance properties of the $DyMn_2O_5$–Mn_3O_4 nanoparticle composite have been experimentally investigated. Two magnetic transitions at temperatures of $T_1 \approx 65$ K and $T_2 \approx 230$ K have been established; the T_1 value differs from the temperatures of the transitions in the initial materials, which has been attributed to the interparticle interactions. Temperature T_2 corresponds to the $DyMnO_3$ impurity phase (1 at %). Three microwave absorption peaks have been observed in the magnetic resonance spectrum, which is explained within the model of a magnetically two-phase system. One resonance is attributed to Mn_3O_4, and the other two peaks are attributed to an ensemble of highly anisotropic $DyMn_2O_5$ particles with a random distribution of anisotropy axes.

DOI: 10.1134/S1063784221040137

INTRODUCTION

At present, compounds of the class of complex oxide materials are being intensively studied [1]. Synthesis of the composites based on various oxides makes it possible to obtain both purely magnetic compounds and the compounds belonging to the family of multiferroics.

In addition, great interest is presented by nano- and microcomposites [2]. This is due to the fact that, in inhomogeneous media, which are the interfaces of materials, the symmetry with respect to the inversion of space and time is broken [3]. These conditions predetermine the coupling between the magnetic and electric subsystems. One of these directions of development is the creation of solid solutions of magnets and ferroelectrics, for example, in the $BiFeO_3$–$PbTiO_3$ system [4]. In addition, to enhance the interfacial bonding, structured composites can be created by mixing different materials.

In this direction, the promising compounds are manganites and spinel-structure oxides [5]. Noda et al. [6] reported the results of magnetic neutron diffraction study of the magnetic and ferroelectric properties of the RMn_2O_5 (R = Y, Tb, Ho, Er, Tm) family compounds. In these compounds, the colossal magnetoelectric effect is observed, which is attributed to the phase transition from the magnetic incommensurate and weakly ferroelectric phase to the magnetic commensurate and ferroelectric phases. This series should be added with the $DyMn_2O_5$ compound [7], in which a great change in the permittivity in a magnetic field was found. This extraordinary effect is apparently caused by the high sensitivity of the magnetic state in the incommensurate phase to external factors.

Another interesting example is Mn_3O_4 tetragonal spinel. Magnetically, this compound is a noncollinear antiferromagnet below 43 K; as the temperature drops below 39 K, a transition to the incommensurate phase occurs [8]. In this compound, the strong magnetodielectric effect was observed [9, 10] and attributed to the strong spin–orbit coupling of Mn^{3+} ions.

It is a common feature of the above-mentioned compounds that they contain Mn magnetic ions with different valences.

We decided to investigate how the magnetic properties of different multiferroic compounds change when they are used to form a composite.

1. EXPERIMENTAL

Complex oxide samples were synthesized by the solid-phase reaction technique. In the synthesis, stoichiometric amounts of the R_2O_3 and Mn_2O_3 oxides of

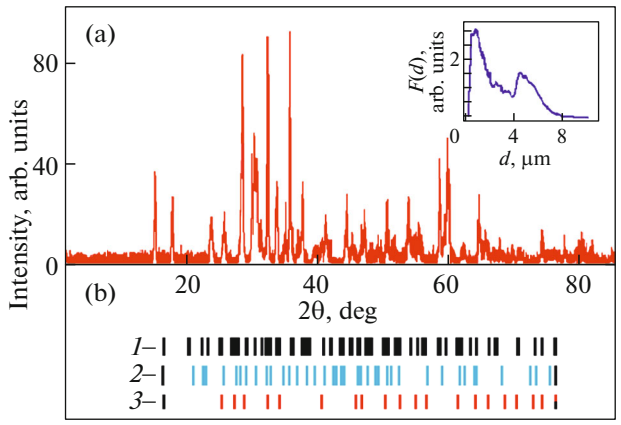

Fig. 1. (a) X-ray diffraction pattern of the composite in the $DyMn_2O_5$–Mn_3O_4 system. (b) Location of the peaks of (*1*) $DyMn_2O_5$–Mn_3O_4, (*2*) $DyMn_2O_5$ ([12], Fig. 1), and (*3*) Mn_3O_4 ([13], Fig. 3). Inset: size distribution function of the particles.

special purity grade were used. The proposed reaction scheme was

$$0.5(Dy_2O_3 + 5Mn_2O_3) \rightarrow DyMn_2O_5 + Mn_3O_4. \quad (1)$$

The mixture was thoroughly ground, mechanically activated in a planetary ball mill, and annealed in five stages at (i) 600, (ii) 700, (iii) 800, (iv) 900, and (v) 1000°C with a total time of 34 h. To improve the homogeneity of the samples, intermediate grinding was performed after each synthesis stage. The composition of the final products was controlled by X-ray fluorescence (XRF). The synthesis of manganites was described in more detail in [11].

The obtained phases were controlled by X-ray diffraction analysis on a Rigaku Miniflex 600 X-ray diffractometer (CuK_α radiation). The size distributions of crystallites were obtained on a CPS Disc centrifuge (ModelDC 24000).

The magnetic characteristics were determined on an MPMS-XL SQUID magnetometer in fields up to 4 MA/m. Electron magnetic resonance (EMR) spectra were recorded on a Bruker E 500 CW EPR spectrometer at a working frequency of $\omega_{MWF} = 9.48$ GHz. The resonance measurements were performed in the temperature range of 80–500 K.

2. EXPERIMENTAL RESULTS

2.1. Structural Data

Figure 1 shows X-ray diffraction data for the synthesized samples. It can be seen in Fig. 1b showing reflection positions that the samples are a mixture of two phases: $DyMn_2O_5$ [12] and Mn_3O_4 [13] (Table 1) in a ratio of 51 : 49; i.e., indeed, we have a mixture of oxides corresponding to formula (1).

The obtained lattice parameters of the oxides forming the composite are given in Table 2 and are consistent with the literature data.

The inset in Fig. 1 shows the size distribution function $f(d)$ of crystallites. For the technique used to synthesize the composite polycrystals, the distribution clearly consists of two maxima, one of them at $d_1 \approx 1.1$ μm and the other at $d_1 \approx 4.8$ μm. It can be seen from the distribution curve that the particle size array is mainly confined to the region of <8 μm. The entire range of particle (block) size distribution extends from 50 nm to 15 μm (individual crystallites).

2.2. Magnetostatic Measurements

It is well-known [15] that, magnetically, $DyMn_2O_5$ single crystals exhibit antiferromagnetic ordering below $T_N \approx 44$ K and undergo transitions at $T = 18$ and 8.4 K, which are related to incommensurate phases. The literature data on the magnetic properties of these nano- and microcomposites are very scarce. In the synthesis of the nanocrystalline Mn_3O_4 compound, the accompanying Mn_2O_3 and/or Mn_5O_8 phases almost always arise [16]. Although their amount is small, they can be in the mixture. Figure 2 shows the magnetization (Fig. 2a) and specific heat (Fig. 2b) data for individual components taken from the literature [9, 17, 18]. It can be seen that, at $T > 45$ K, no features are observed in the temperature dependences of the magnetization and specific heat of the initial compounds.

Figure 3 shows the temperature dependences of the magnetization ($M(T)$) measured in different magnetic fields. It can be seen that the shape of the $M(T)$ curve strongly depends on the measuring field (curves *1*–*4*). In fields of $H \le 0.8$ MA/m, two features at temperatures $T_1 \sim 65$ K and $T_2 \sim 230$ K are observed, where the magnetization decreases; they can be identified as the ordering temperatures of the low- and high-temperature magnetic phases. The transition at tempera-

Table 1. Identification of phases in the synthesized composite

Chemical formula	Space group	Data on phase detection	DB card number
$DyMn_2O_5$	55 Pbam (Orthorhombic)	DD (PDF-2/Release 2013 RDB)	01-072-1696
Mn_3O_4	141-I41/amd,choice-2 (Tetragonal)	DD (PDF-2/Release 2013 RDB)	01-071-6262

Table 2. Lattice parameters of the magnetic phases in the composite

Compound	a, Å	b, Å	c, Å	Alpha, deg	Beta, deg	Gamma, deg	V, Å^3
$DyMn_2O_5$ [12]	7.377	8.523	5.702	90.000000	90.000000	90.000000	358.5
Mn_3O_4 [14]	5.759	5.759	9.456	90.000000	90.000000	90.000000	313.68

ture T_1 is sharp, while the transition at temperature T_2 is diffuse and occupies the region of $T > 50$ K. As the measuring field increases, the temperature range of the transition increases and, in a measuring field of $H = 8$ MA/m, a high-temperature transition is no longer visible. Thus, the $M(T)$ curve is a sum of several terms and the high-temperature phase is more strongly affected by the external magnetic field. For the low-temperature phase, temperatures T_1 of the transition were found to be 63, 65, 68, and 76 K in magnetic fields of $H = 40$, 400, 800, and 4000 kA/m, respectively. The shape of the field dependences of the magnetization ($M(H)$) strongly depends on the measuring temperature. At the liquid helium temperature (Fig. 4) in fields of $H \le 200$ kA/m, a hysteresis loop is observed, but there is no saturation to a field of $H =$ 4 MA/m (inset in Fig. 4). As the temperature increases to $T = 65$ K, a weak hysteresis is still observed (curve *1* in Fig. 4); at temperatures of $T \ge 70$ K, the $M(H)$ curves are hysteresis-free (curve *2*, Fig. 4). However, up to room temperatures, the magnetization does not saturate with an increase in the field to 4 MA/m; the $M(H)$ curves have a slight slope, which decreases with increasing temperature. Temperature T_1 determines the region of existence of the hysteresis from above, while temperature T_2 in no way manifests itself in the field dependences.

2.3. Magnetic Resonance

The magnetic resonance measurements can yield additional data for understanding the behavior of the magnetic phases in the synthesized composite. The resonance absorption was measured in the temperature range of $T = 80 - 450$ K. Figure 5 shows a typical resonance absorption spectrum at $T = 300$ K. The obtained experimental resonance curve (open symbols) has a complex shape. We approximated this curve by a sum of components of the Lorentzian absorption line derivatives (curves *1*–*3*); the best fit is shown in Fig. 5 (curve *4*). It can be seen that the result obtained is quite well. For all three lines from Fig. 5, Fig. 6a shows the temperature dependences of the resonance fields H_r. Note that line *1* tends to a decrease in the resonance field with increasing temperature. Line *2* shows a weak temperature dependence of H_r, with a slight increase with increasing temperature. Line *3*

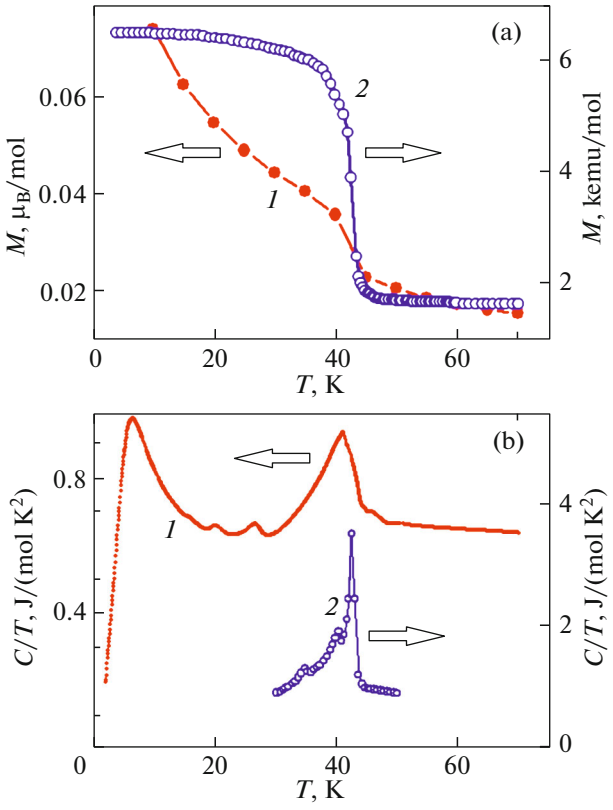

Fig. 2. Temperature dependences of (a) magnetization and (b) specific heat. Curves *1* and *2* correspond to the polycrystalline $DyMn_2O_5$ and Mn_3O_4 compounds, respectively. (a, b) Curves *1* are taken from [17] and [18], respectively. (a, b) Curves *2* are taken from [9].

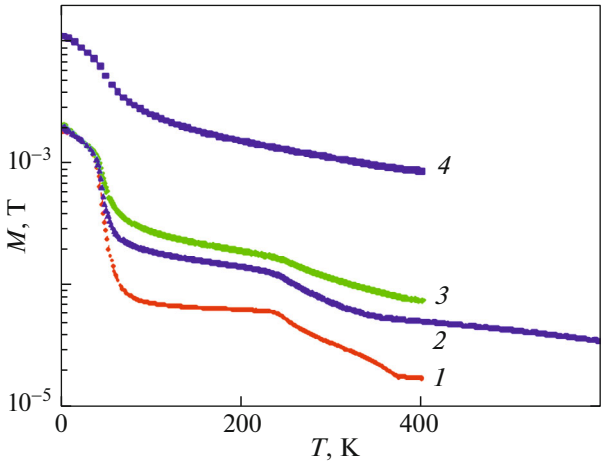

Fig. 3. Temperature dependences of magnetization of the $DyMn_2O_5$–Mn_3O_4 composite. $H =$ (*1*) 0.04, (*2*) 0.4, (*3*) 0.8, and (*4*) 4 MA/m.

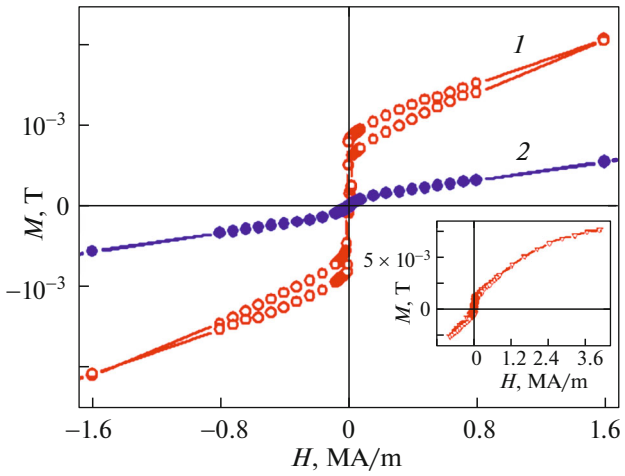

Fig. 4. Field dependences of magnetization at (*1*, *2*) $T = 20$ and 70 K. Inset: magnetization loop at $T = 4.2$ K obtained in fields of up to $H = 4$ MA/m.

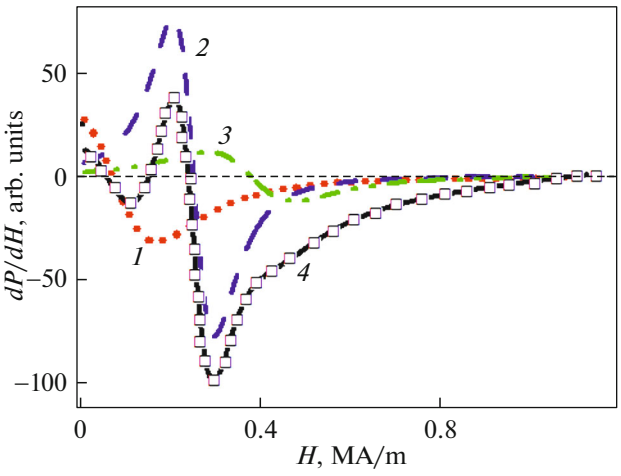

Fig. 5. Magnetic resonance spectrum. Open symbols show the experiment. (*1*–*3*) Decomposition into component lines. (*4*) Sum of the components. $T = 300$ K.

shows the strongest temperature dependence of the resonance field.

The behavior of the linewidths (ΔH_{pp}) (Fig. 6b) is characterized by the fact that the width of line *2* monotonically decreases with increasing temperature, while the ΔH_{pp} value for lines *1* and *3* have a minimum in the temperature dependence. In this case, line *1* in the range of $T > 200$ K shows a noticeable increase in the ΔH_{pp} value. The temperature dependences of the intensities J calculated as areas under the corresponding absorption lines [19] are presented in Fig. 6c. Here, there is a noticeable increase in the intensity of line *1* at temperatures of $T > 250$ K.

3. RESULTS AND DISCUSSION

It follows from the above data that, for the $DyMn_2O_5$ and Mn_3O_4 single crystals, the transition temperatures fall into approximately the same temperature range of 40–50 K. If we assume that the synthesized composite is a simple mixture of these compounds, then the modification of the magnetic properties will mainly be due to the interaction of grains across their interfaces. This manifests itself as the absence of features in the temperature dependence of the magnetization at temperatures below the ordering temperatures of the initial materials. When the particle size changes, the Curie temperature changes as well, but it still cannot be higher than that of the bulk material [20]. In our case, the transition temperature increased by about 15 K, which is indicative of the activation of an additional mechanism. It can be assumed that a mechanism is the interaction across the interface between neighboring particles, since both the coordination number of magnetic ions and the exchange between neighboring particles can change.

It was previously established [21] that, at the transition to the nanoscale, $DyMn_2O_5$ particles ~7 nm in size in a porous silicon matrix exhibit the superparamagnetic behavior with a blocking temperature around 14 K. In nanorods [22] with a ratio of $D/L_S \approx 2$ (D is the rod diameter and L_S is the rod length) at $L_S =$ 46, 84, and 212 nm, the temperatures of the transition to the antiferromagnetic state are $T_N \approx 42$, 42, and 50 K. In addition, it was found that the saturation magnetization and the coercivity decrease with increasing L_S value. For Mn_3O_4 nanoparticles [23] 15–25 nm in size, the temperature of the transition to the magnetically ordered state does not change. In our case, the particle size is $d > 1$ μm, so that the size spread does not affect the magnetic properties. It is well-known that, with an increase in the size of small particles, at certain critical size d_c, the magnetization saturates, e.g., for metallic cobalt particles, the size is $d_c \sim 0.15$ μm [24]; for the $La_{2/3}Sr_{1/3}MnO_3$ manganite particles, this size is 0.2 μm [25]. Here, the main effect is the suppression of low-temperature transitions due to the spin disordering on the nanoparticle surface. However, ordering temperature T_1 for the synthesized $DyMn_2O_5$–Mn_3O_4 composite, being a magnetic transition temperature for none of the initial components, nevertheless correlates with the mode softening temperature in the infrared range for the rare-earth RMn_2O_5 compounds due to the spin–phonon coupling [26]. The authors interpreted this result as a manifestation of local lattice distortions, which is important for the occurrence of the ferroelectric polarization and the magnetoelectric effect.

The high-temperature transition at T_2 is not explained by the presence of only $DyMn_2O_5$ and Mn_3O_4 particles. In addition, note the weak magnetization at temperatures of $T > 60$ K and the strong mag-

netic field dependence as compared with the low-temperature phases. There is, apparently, a small amount of one more phase, which is masked by the main phases. If we relate to the high-temperature transition temperature ($T_2 \sim 230$ K), then the transition temperature of the disordered rare-earth $RE_{1-x}B_xMnO_3$ manganites (where B is a divalent alkaline-earth element) falls into this region, where the spin-glass-like state can be implemented [27]. In these compounds, disordering of manganese ions can occur due to the incorporation of B^{2+} ions, which leads to the formation of Mn^{4+} ions. However, in the case of small particles, the mixed valence of manganese is induced by the oxygen nonstoichiometry. As was shown in [28], the formation of a rare-earth manganite can occur according to the scheme

$$DyMn_2O_5 = DyMnO_3 + (1/3)\,Mn_3O_4 + (2/3)\,O. \quad (2)$$

This reaction explains the experimental ratio between the $DyMn_2O_5$ and Mn_3O_4 phases in the final product.

If we assume that the composite is a mixture of two magnetic substances, $DyMn_2O_5$ and Mn_3O_4, with an impurity of some third phase, then the question of identifying the peaks in the microwave absorption spectrum (Fig. 5) arises. It is well-known that the microwave radiation power absorbed at the resonance is determined by the relation [29]

$$P = (\omega\chi'' h^2)/2, \quad (3)$$

where ω is the resonance frequency, χ'' is the imaginary part of the magnetic susceptibility tensor, and h is the amplitude of the magnetic field of microwave radiation.

When studying the resonance properties of the composite systems with the weak interparticle coupling, assuming the linewidth of an individual particle to be extremely narrow, one can use the approach developed to describe inhomogeneous systems, in particular, polycrystalline samples [30]:

$$\chi''(\omega, H) = \{\pi M_o \iint \delta[H - H_r(\omega, \theta, \varphi)]\sin\theta d\theta d\varphi\}/4. \quad (4)$$

Here, H_r is the resonance field of a particle, M_o is the saturation magnetization, $\delta(x)$ is the Dirac delta function, and the integration is made over the total solid angle.

It follows from a comparison of the resonance fields in our experiment with the literature data for Mn_3O_4 nanoparticles [31] that line *2* in Fig. 5 falls into the field range typical of Mn_3O_4 nanoparticles and can be identified as corresponding to this compound. Since we deal with an ensemble of particles with the averaged parameters, the fine structure does not manifest itself. The data of [32] allow one to conclude that the magnetic resonance is mainly determined by the subsystem of Mn^{2+} ions.

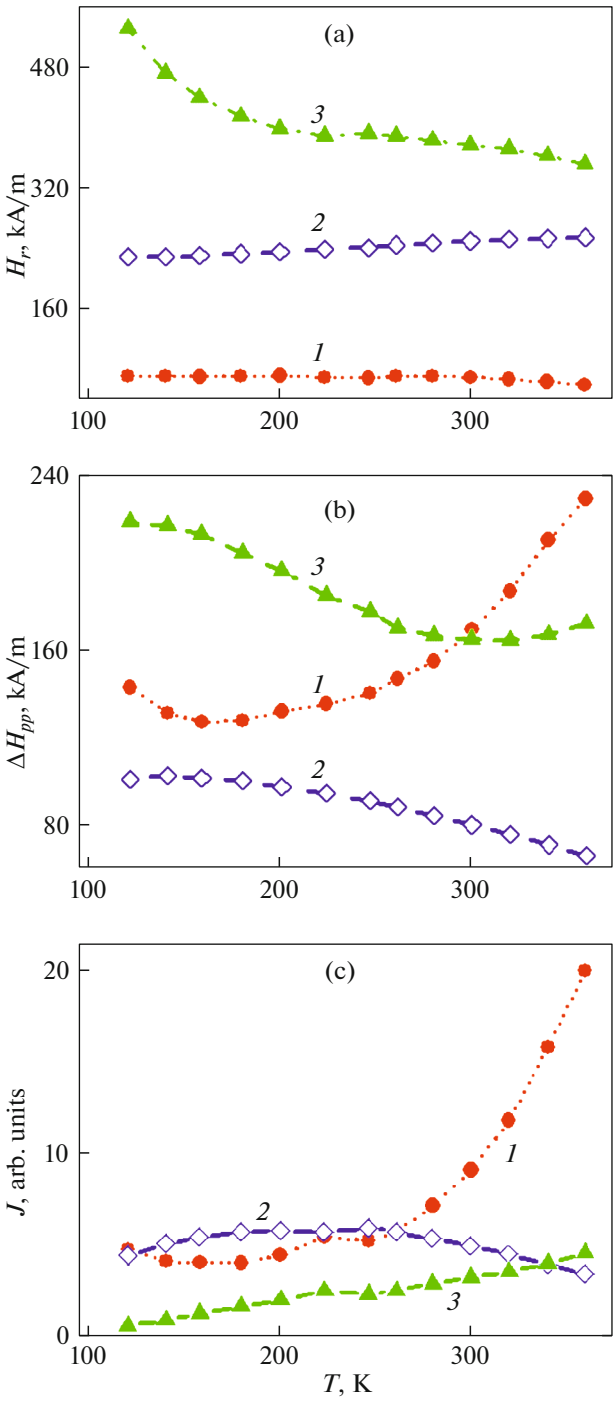

Fig. 6. Temperature dependences of the parameters of the resonance curves. (a) Resonance field, (b) magnetic resonance linewidths, and (c) intensities of the absorption lines. The curves are numbered according to the lines in Fig. 5.

The resonance from the possible $DyMnO_3$ phase should not be observed for two reasons. First, since manganese is included in the trivalent state, it has a

significant initial splitting [29] and the resonance absorption at a microwave frequency of ω_{MWF} = 9.48 GHz is improbable. Nevertheless, in the disordered ceramic systems of the $La_{1-x}Sr_xMn_{1-y}Zn_yO_3$ type, the magnetic resonance from superparamagnetic particles in the paramagnetic phase from ferromagnetically correlated spins was observed [33]. Second, the amount of this phase should be no more than 1 at %, which is certainly insufficient for a signal comparable in intensity with the signals of other phases (Fig. 6c).

For the $DyMn_2O_5$ compound (the orthorhombic symmetry), we should note the high magnetic anisotropy with the easy magnetization direction along the **b** axis [34]. As is known [35], in polycrystalline systems (crystallites have the uniaxial magnetic anisotropy), the magnetic resonance spectrum depends on the ratio between Zeeman energy E_Z and magnetic anisotropy energy E_A. If the magnetic anisotropy energy significantly exceeds the Zeeman energy, then the spectrum has a complex form and, as a rule, consists of two peaks. In [35], based on Eq. (4), the shape of the resonance absorption spectrum of an ensemble of particles with a random distribution of the anisotropy axes was numerically calculated as a function of the energy ratio E_A/E_Z. One of the peaks is determined by the fraction of particles with the predominant direction of the external magnetic field along the easy axis, and the other is determined by the fraction of particles with the external magnetic field directed along the hard axis. According to the calculated data, the intensity of the microwave absorption peaks is pumped over upon temperature variation. In our case, we have a qualitative agreement between the results of such a calculation and the experiment.

4. CONCLUSIONS

In this study, it was established that a system of bound particles is formed in the $DyMn_2O_5$–Mn_3O_4 composite synthesized for the first time. This manifests itself in the difference between the magnetic properties of the composite and initial materials.

—It was found that, at low temperatures, the magnetic behavior cannot be described by algebraic summation of curves of the initial materials; in addition, the temperature of the transition to the disordered state increases ($T \sim 65$ K). Oxygen nonstoichiometry causes a small admixture of a magnetic phase (presumably, $DyMnO_3$) with an ordering temperature of $T \sim 230$ K.

—The magnetic resonance data clearly indicate the presence of an ensemble of Mn_3O_4 particles.

—For the $DyMn_2O_5$ phase, the absorption spectrum is related to the magnetic resonance in an ensemble of strongly anisotropic particles with a random distribution of the anisotropy axes.

In this last case, questions about the value of the magnetic anisotropy in grains and the interparticle coupling at the grain boundaries remain open.

ACKNOWLEDGMENTS

The measurements of the magnetic resonance spectra were performed on the equipment of the Center for Collective Use of Krasnoyarsk Scientific Center, Siberian Branch, Russian Academy of Sciences.

FUNDING

This study was supported by the Ministry of Education and Science of the Republic of Kazakhstan (project no. 05130165) and within the framework of a state assignment of the Ministry of Science and Higher Education of the Russian Federation (theme no. FSRZ-2020-0011) in the framework of the Cooperation Agreement between Siberian Federal University, Kirensky Institute of Physics, and Kazakh National Women's Teacher Training University.

CONFLICT OF INTEREST

The authors declare that they have no conflicts of interest.

REFERENCES

1. N. A. Spaldin, S.-W. Cheong, and R. Ramesh, Phys. Today **63**, 38 (2010).
2. "Why Nanoscale Ferroelectrics and Multiferroics?" in *Nanoscale Ferroelectrics and Multiferroics: Key Processing and Characterization Issues, and Nanoscale Effects*, Eds. by M. Algueró, J. M. Gregg, and L. Mitoseriu (Wiley, Chichester, 2016), Vol. 1.
3. A. P. Pyatakov and A. K. Zvezdin, Phys.-Usp. **55**, 557 (2012). https://doi.org/10.3367/UFNe.0182.201206b.0593
4. H. Amorín, C. Correas, C. M. Fernández-Posada, O. Peña, A. Castro, and M. Algueró, J. Appl. Phys. **115**, 104104 (2014).
5. K. F. Wang, J.-M. Liu, and Z. F. Ren, Adv. Phys. **58**, 321 (2009).
6. Y. Noda, H. Kimura, M. Fukunaga, S. Kobayashi, I. Kagomiya, and K. Kohn, J. Phys.: Condens. Matter **20**, 434206 (2008).
7. N. Hur, S. Park, S. Guha, and S.-W. Cheong, Phys. Rev. Lett. **3**, 107207 (2004).
8. C. Kim, E. Jo, B. Kang, S. L. Kwon, and S. Lee, Phys. Rev. B **86**, 224420 (2012).
9. R. Tackett and G. Lawes, Phys. Rev. B **76**, 024409 (2007).
10. T. Suzuki and T. Katsufuji, Phys. Rev. B **77**, 220402 (2008).
11. M. M. Mataev, S. Saxena, G. S. Patrin, Zh. Y. Tursinova, A. T. Kezdikbayeva, M. A. Nurbekova, and G. U. Baitasheva, Orient. J. Chem. **34**, 1312 (2018).
12. S. C. Abrahams and J. L. Bernstein, J. Chem. Phys. **46**, 3776 (1967).

13. E. Winkler and R. D. Zysler, Phys. Rev. B **70**, 174406 (2004).
14. H. Dhaouadi, O. Ghodbane, F. Hosni, and F. Touati, Int. Scholarly Res. Not. **2012**, 706398 (2012). https://doi.org/10.5402/2012/706398
15. C. Wilkinson, F. Sinclair, P. Gardner, J. B. Forsyth, and B. M. R. Wankly, J. Phys. C: Solid State Phys. **14**, 1671 (2008).
16. L. Dimesso, L. Heider, and H. Hahn, Solid State Ionics **123**, 39 (1999).
17. T.-C. Han and J. G. Lin, J. Appl. Phys. **99**, 08J508 (2006).
18. Z. Y. Zhao, M. F. Liu, X. Li, L. Lin, Z. B. Yan, S. Dong, and J.-M. Liu, Sci. Rep. **4**, 3984 (2014).
19. Ch. P. Poole, Jr., *Electron Spin Resonance* (Wiley, New York, 1967).
20. Yu. A. Koksharov, "Magnetism of nanoparticles: Effects of size, shape and interaction," in *Magnetic Nanoparticles*, Ed. by S. P. Gubin (Wiley, Weinheim, 2009), p. 197.
21. T. Tajiri, Y. Ando, H. Deguchi, M. Mito, and A. Kohno, Phys. Procedia **75**, 1181 (2015).
22. Y. H. Tung, Ch.-Ch. Yang, T.-W. Hsu, Ch.-W. Kao, and Y. Y. Chen, AIP Adv. **7**, 055830 (2017).
23. R. Regmi, R. Tackett, and G. Lawes, J. Magn. Magn. Mater. **321**, 2296 (2009).
24. V. O. Vas'kovskiy, G. S. Patrin, D. A. Velikanov, A. V. Svalov, P. A. Savin, A. A. Yuvchenko, and N. N. Shchegoleva, Phys. Solid State **49**, 302 (2007). https://doi.org/10.1134/S1063783407020199
25. L. Balcells, J. Fontcuberta, B. Martínez, and X. Obrador, Phys. Rev. B **58**, R14697 (1998).
26. J. Cao, L. I. Vergara, J. L. Musfeldt, A. P. Litvinchuk, Y. J. Wang, S. Park, and S.-W. Cheong, Phys. Rev. B **78**, 064307 (2008).
27. E. Dagotto, *Nanoscale Phase Separation and Colossal Magneto-Resistance. The Physics of Manganites and Related Compounds* (Springer, Berlin, 2003), Chap. 13.
28. L. B. Vedmid', V. F. Balakirev, A. M. Yankin, Yu. V. Golikov, and O. M. Fedorova, Inorg. Mater. **44**, 316 (2008). https://doi.org/10.1134/S0020168508030199
29. A. Abragam and B. Bleaney, *Electron Paramagnetic Resonance of Transition Ions* (Clarendon, Oxford, 1970).
30. A. G. Gurevich and G. A. Melkov, *Magnetization Oscillations and Waves* (CRC, New York, 1996).
31. Z. Durmus, A. Baykal, H. Kavas, M. Direkci, and M. S. Toprak, Polyhedron **28**, 2119 (2009).
32. H. Dhaouadi, O. Ghodbane, F. Hosni, and F. Touati, ISRN Spectrosc. **1** (2012).
33. R. M. Eremina, K. R. Sharipov, L. V. Mingalieva, and A. G. Badelin, JETP Lett. **98**, 848 (2014). https://doi.org/10.1134/S0021364013250115
34. N. Hur, S. Park, P.A. Sharma, S. Guha, and S.-W. Cheong, Phys. Rev. Lett. **93**, 107207 (2004).
35. A. Sukhov, K. D. Usadel, and U. Nowak, J. Magn. Magn. Mater. **320**, 31 (2008).

Translated by E. Bondareva